Theory of a Forward-Biased Diffused-Junction P-L-N Rectifier—Part I: Exact Numerical Solutions

SEOK CHEOW CHOO, MEMBER, IEEE

Abstract—Exact numerical solutions have been obtained for a forward-biased diffused-junction n^+-p-p^+ silicon rectifier operating from low to high injection levels. The results indicate that under high-level injection conditions, there exists a quasi-neutral region (i.e., a region wherein the electron and hole concentrations are very nearly equal) in the device which is not confined to the lightly doped p-base region but stretches into the diffused n^+ region as the injection level increases. For the impurity profile and the Shockley-Read-Hall recombination model used, it is additionally found that the quasi-Fermi potentials for both electrons and holes are constant across a large portion of the diffused region adjoining the quasi-neutral or "effective base" region. The most significant finding, however, is that at the boundary between the effective base region and the diffused region, the hole current varies more or less directly as the carrier concentration, in contrast to the situation in a step-junction rectifier where the minority carrier current in the heavily doped regions varies as the square of the carrier concentration at the base edge. A simple analysis shows that this linear relationship can be related to the constant quasi-Fermi potentials across the diffused region.

As a consequence of the aforementioned linear relationship, the injection efficiency of the diffused junction is roughly independent of the injection or current levels. It may be high or low depending on whether the concentration of recombination centers in the diffused region is small or large compared to that in the base region. This is unlike the situation in a step junction where the injection efficiency would be initially high and then degrade, as the current increases.

Nomenclature

B	$=(\mu_n-\mu_p)/(\mu_n+\mu_p)$.
B'	Defined by (14).
c_n, c_p	Capture rate of electrons or holes.
D_n, D_p	Diffusion coefficient of electrons or holes.
E	Electric field.
J_b	Recombination current density in the effective base region, defined by (10).
J_n, J_p, J_t	Electron, hole, and total current density.
k	Boltzmann's constant.
L_a, L_n	Ambipolar diffusion length, electron diffusion length.
N_A, N_D, N_I	Acceptor, donor, and net impurity concentrations ($N_I=\lvert N_D-N_A\rvert$).
N_t	Concentration of recombination centers.
N^+, P^+	Equilibrium electron and hole concentrations in the uniformly doped n^+ and p^+ regions, respectively.
n, p	Electron and hole concentrations.
n_1, p_1	Equilibrium electron and hole concentrations when Fermi level coincides with energy level of recombination centers.
n_i	Intrinsic carrier concentration.
n_p	Equilibrium electron concentration in p base.
Δn	Excess electron concentration.
q	Electronic charge.
T	Absolute temperature (=300 K).
U	Net rate of recombination of electrons and holes.
V_A	Applied voltage.
V_b	Base voltage, given by $-\int_{W_1'}^{W_2'} E dx$.
V_{j1}	$=(\psi_{d1}{}^0-\psi_{d1})$.
V_{j2}	$=(\psi_{d2}{}^0-\psi_{d2})$.
V_t	Thermal voltage (kT/q).
W_0, W_1, W_2, W_3	Location of boundary between uniformly doped n^+ and diffused regions, location of n-p transition, location of p-p^+ transition, and total width of device (see Fig. 1).
W_1'	Boundary between diffused region and effective base region under high-level conditions, defined as the position where the electron and hole concentrations have converged to within 1 percent of one another.
W_1''	Location of the boundary between the uniformly doped p base (i.e., where $N_A-N_D=1\times10^{14}$ cm^{-4} in Fig. 1) and the compensated p region (i.e., where $N_A-N_D<1\times10^{14}$ cm^{-3}).
W_2', W_2*	Boundaries where both Boltzmann's relations and quasi-neutrality condition are satisfied, located, respectively, on the lightly doped side and the heavily doped side of p-p^+ junction.
x	Spatial coordinate.
δ	Damping factor used in modified form of De Mari's algorithm.
ϵ	Permittivity of the semiconductor equals 11.7.
μ_n, μ_p	Electron or hole mobility.
μ_{n0}, μ_{p0}	Electron or hole mobility in the absence of carrier–carrier scattering.

Manuscript received October 26, 1971; revised February 17, 1972.
The author is with Westinghouse Research Laboratories, Pittsburgh, Pa. 15235.

μ_{np} Carrier–carrier scattering mobility.
τ Carrier lifetime in the effective base region, under high-level conditions.
τ_{n0} $=(N_t c_n)^{-1}$.
τ_{p0} $=(N_t c_p)^{-1}$.
ϕ_n, ϕ_p Electron or hole quasi-Fermi potential.
ψ Electrostatic potential.
ψ_d Diffusion or barrier potential across the whole device.
ψ_{d1} Barrier potential across the diffused region $(=\psi(0)-\psi(W_1'))$.
ψ_{d2} Barrier potential across the p^+-p junction $(=\psi(W_2')-\psi(W_2^*))$.
ψ_{d1}^0, ψ_{d2}^0 Equilibrium barrier potential across the diffused junction, or across the p^+-p junction.

Introduction

THE theory of a forward-biased p-L-n rectifier operating at high current densities has been extensively treated in the literature [1]–[4]. However, all the treatments presented thus far have used the step-junction approximation for both the p-n junction and the high-low junction. While this approximation is a reasonable representation of alloyed junctions, it clearly cannot be applied in general to diffused junctions of present day devices. Despite its obvious limitations, the step-junction theory provided a necessary first step toward the development of a more general rectifier theory, and for this reason, we have recently used [5] the numerical analysis approach to carry out a rigorous examination of the validity of this theory, particularly in regard to the two key assumptions on which it rests, namely, the assumptions of quasi-neutrality and of the Boltzmann junction relationships.

The present paper is a sequel to an earlier paper [5]. Exact numerical solutions will be presented here that give a complete description of the static behavior of a forward-biased diffused-junction p-L-n rectifier. The purpose of obtaining these exact solutions is twofold: first, to achieve a detailed understanding of the internal behavior of the diffused-junction rectifier, and second, to use the solutions as a guide in the development of an approximate analytical theory for this type of rectifier.[1]

The device studied is a single-diffused silicon high-power n^+-p-p^+ rectifier. A single-diffused structure has been chosen in order to focus our attention on the role played by the diffused n^+-p junction in determining the device characteristics. The solutions obtained range from very low to very high injection levels, up to 10^{18} cm^{-3}. Some of the low injection level solutions have previously been reported [6]. They are included here for the sake of completeness.

[1] Although such a theory has been successfully developed, it will not be given here as it will form the subject of a subsequent paper.

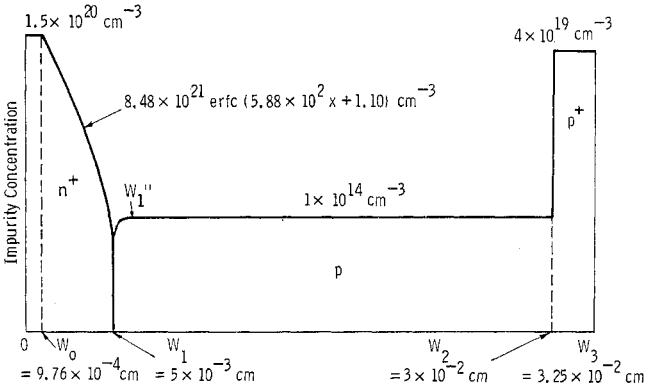

Fig. 1. One-dimensional n^+-p-p^+ rectifier structure.

Mathematical and Physical Model

The system of equations governing the steady-state flow of electrons and holes is well known. With the assumptions of nondegeneracy and absence of carrier trapping effects, it is given in one-dimensional form as follows:

$$J_n = -q\mu_n(n\cdot d\psi/dx - V_t\cdot dn/dx) \quad (1)$$

$$J_p = -q\mu_p(p\cdot d\psi/dx + V_t\cdot dp/dx) \quad (2)$$

$$dJ_n/dx = -dJ_p/dx = qU \quad (3)$$

$$d^2\psi/dx^2 = -(q/\epsilon)(p - n + N_D - N_A). \quad (4)$$

We assume that the device is bounded by a pair of infinite recombination-velocity contacts located at $x=0$ and $x=W_3$. Moreover, we solve the problem for given values of applied voltage, so that the boundary conditions on ψ are as follows: $\psi(0)=0$ and $\psi(W_3)=V_A-\psi_d$.

The device studied is a Westinghouse Type 790 n^+-p-p^+ rectifier with a junction area of 2 cm^2. Its impurity profile has been determined from spreading resistance measurements [7], and is closely approximated by the distribution in Fig. 1.

In our numerical solutions, carrier mobilities are assumed to vary with the impurity concentration according to the expression given by Scharfetter and Gummel [8]. In addition, the effects of carrier–carrier (c-c) scattering [2], [3], [9], important at high injection levels, are included by using Fletcher's expression [2] and are described by the parameter μ_{np} below. As in [5], carrier heating effects are ignored since they are unimportant for a forward-biased rectifier.

The recombination rate U in (3) is specified by invoking the Shockley–Read–Hall model [10]. The concentrations of recombination centers in the uniformly doped n^+ and p^+ regions shown in Fig. 1 are chosen so that they yield the small diffusion lengths that have been found [11], [12] for the alloyed regions of rectifiers. In the p region, the concentration is made sufficiently large so that it gives an ambipolar diffusion length which is comparable to the width of this region [4]. The choice of the concentration in the diffused region is arbitrary due to the absence of any experimental data to guide us. However, because this is the first treatment of the dif-

fused-junction rectifier, we have chosen to concentrate on the simplest case by assuming that the concentration in the diffused region is the same as that in the p region, although, for purposes of comparison, we shall also present, toward the end of this paper, some of the solutions obtained for the case where these concentrations are different.

The main physical parameters characterizing the structure then are the following.

Mobilities

$$\mu_n = (\mu_{n0}^{-1} + \mu_{np}^{-1})^{-1} \tag{5}$$

$$\mu_p = (\mu_{p0}^{-1} + \mu_{np}^{-1})^{-1} \tag{6}$$

where μ_{n0} and μ_{p0} are functions of N_I as given by Scharfetter and Gummel [8], and

$$\mu_{np} = 2.00 \times 10^{17} T^{3/2} \{(np)^{1/2} \cdot \ln [1 + 8.28 \times 10^8 T^2 (np)^{-1/3}]\}^{-1} \text{ cm}^2/\text{V}\cdot\text{s}. \tag{7}$$

Recombination Model

For a Shockley–Read–Hall model

$$U = \frac{pn - n_i^2}{\tau_{p0}(n + n_1) + \tau_{n0}(p + p_1)} \tag{8}$$

where the parameters of the model are assumed to have the following values: $n_1 = p_1 = n_i$ and $\tau_{n0}/\tau_{p0} = 10$ for all regions shown in Fig. 1; $\tau_{p0} = 2 \times 10^{-6}$ s for the n^+ diffused and p region, 4.5×10^{-8} s for the uniformly doped portion of the n^+ region, and 2×10^{-10} s for the p^+ region.

Numerical Method of Solution

The numerical method initially used in the present work for solving (1)–(4) was based on that proposed by Gummel [13] and De Mari [14]. The iterative scheme employed is shown in Table I, and it is readily recognized as the one given by De Mari, if the factor δ associated with the recombination-rate equation is set equal to zero. This factor was introduced in order to allow for a gradual change in U from one iteration to the next, for it was found very early in this work that, while the original De Mari algorithm with $\delta = 0$ worked well for cases where the effects of recombination are slight to moderate throughout the device, it failed in our case where strong recombination occurs in the p^+ region.[2] The use of the "damping" factor improved the situation by allowing us to obtain accurate solutions up to bias conditions where the contribution of the recombination current in the p^+ region to the total current across the device is negligible. However, it too failed at larger bias voltages when this contribution becomes significant.

The foregoing remarks apply to cases where we have deliberately excluded from consideration the effects of c-c scattering. The inclusion of c-c scattering further reduces the upper limit of the bias range where the above method can be applied, since the effect of c-c scattering is to decrease the ambipolar diffusion length in the p region, thereby increasing the width to diffusion length ratio of this region.

Various other remedies were tried on De Mari's algorithm. For example, convergence on ψ was found before allowing U to change or vice versa. All of these techniques improved the situation slightly, but were unable to significantly extend the range of usefulness of the algorithm, even in the absence of c-c scattering.

It became clear then that a different method had to be developed. The approach that was adopted, and which has proven successful in overcoming all of the difficulties associated with recombination, is described in [16]—it is rather similar to that described in some detail by Caughey [17]. The method has been applied to a large variety of problems, and in every case it has worked. For example, it can tackle with ease the effects

TABLE I
MODIFIED FORM OF DE MARI'S ITERATIVE SCHEME

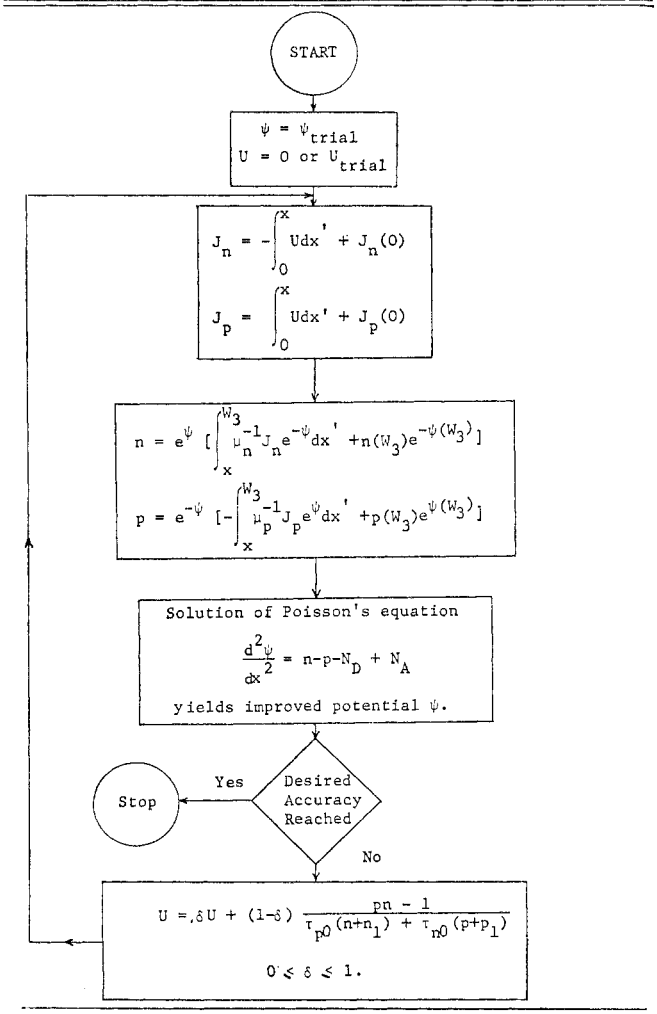

Note: All quantities shown are normalized in accordance with Table II.

[2] A useful criterion we found for assessing the effect of recombination is to consider the width to diffusion length ratio in a given region. If this is very large compared to unity, as in the case of the p^+ region, then strong recombination prevails. But, if it is comparable to unity, we have moderate recombination—this was the case treated by Arandjelovic [15], and explains why he did not encounter any difficulty with his algorithm which is similar to De Mari's.

of c-c scattering, as well as cases where the concentrations of recombination centers in the diffused n^+ region, the p region, and the p^+ region have been successively increased from those given earlier by at least an order of magnitude. All of the numerical results to be presented were obtained by this method.

Numerical Results

The results of the numerical calculations are shown in Figs. 2–8. Figs. 2–6 refer to solutions obtained for V_A from 2 to $37.5\,V_t$ by ignoring the presence of c-c scattering, while Figs. 7 and 8 show the changes that occur when c-c scattering is taken into account at $V_A = 35$ and $37.5\,V_t$, respectively. (Note that, unless otherwise stated, all the quantities shown in all the figures in this paper are normalized in accordance with Table II.)

We shall first examine the solutions in terms of the contributions of the various regions in the device to the total current and applied voltage, since this would enable us to determine the relative importance of each region in determining the overall characteristics of the device. We note that at $V_A = 2\,V_t$ (Fig. 2), the lightly doped base region is under low-level injection condition and all of the applied voltage falls across the diffused junction. The large drop in the electron current across this junction, corresponding to the rise in the hole current, indicates that all the current arises from space-charge recombination.[3] As V_A is increased to $10\,V_t$ (Fig. 3), low-level conditions still prevail in the base. However, while space-charge recombination at the diffused junction remains significant, the main contribution to the total current is due to recombination in the base. At $V_A = 20\,V_t$ (Fig. 4), the base is under medium-level injection, when the injected carrier concentration becomes comparable to the base impurity concentration. Base recombination now accounts for all the current. As yet there is no significant modulation of the p^+-p junction potential.

Base recombination continues to dominate the current, as the base enters into high-level injection condition at $V_A = 30\,V_t$ (Fig. 5). Some of the applied voltage is now taken up by the p^+-p junction. At $V_A = 37.5\,V_t$ (Fig. 6), the carrier concentrations in the base approach 10^{18} cm^{-3}. Further reduction in the p^+-p junction potential has occurred, along with a voltage buildup in the base. In addition, the contribution of the recombination current from the p^+ region has become comparable to the base current. This trend continues at still larger bias voltages corresponding to injection levels exceeding 10^{18} cm^{-3}. Solutions at these bias levels were not obtained, however, since it is obvious that at such high injection levels the nondegeneracy assumption can no longer be justified.

As is well known, the presence of c-c scattering tends to reduce the carrier mobilities in silicon at injection levels greater than 10^{16} cm^{-3} [3]. From Figs. 7 and 8 it can be seen that the net result of the inclusion of this scattering mechanism is an overall reduction of carrier concentrations, the reduction being more drastic for $V_A = 37.5\,V_t$ than for $V_A = 35\,V_t$. The decrease in carrier concentrations means a smaller total current, and, for a given applied voltage, an increase in the voltage drop across the base at the expense of those across the junctions.

There are two important features common to all the solutions referred to above, namely, the constancy of the quasi-Fermi potentials relative to the electrostatic potential through a major portion of the diffused region adjoining the base, and the fact that the quasi-neutrality condition applies throughout the base. The second feature is similar to what we find in a step-junction p-L-n rectifier. But, unlike the latter, if we consider the effective base region under high-level conditions as the region where $n \simeq p$, we see from Figs. 5 and 6 that this region does not remain fixed in width, but stretches into the diffused region as the injection level increases.

However, the single most important difference between the present structure and the step-junction rectifier lies in the relationship of the recombination current in the diffused region to that in the base under high-level conditions. As shown in Figs. 5 and 6 the ratio of these two currents is about 1 to 10, but what is significant is that this ratio is practically constant, regardless of the current or injection level. Since the base recombination current varies linearly with the base carrier concentration, this indicates that the diffused-region recombination current is linearly related to the carrier concentration at the edge of the effective base region—a situation which is in marked contrast to that in a step junction where the diffusion or recombination current in the heavily doped region varies as the square of the carrier concentration at the base edge [4]. There are broad implications to this finding, but a discussion of these is deferred to a later section.

Comparison of Numerical and Analytical Solutions

Base Region

Low-Level Condition: Under low-level conditions, the situation is identical to that in a step-junction rectifier. The numerical solutions verify that the injected carrier distribution for $W_1'' \leq x \leq W_2'$ is accurately given by the well-known field-free approximation [18], and that the injected carrier concentration at the edge of the lightly doped base region is also correctly given by the simple Boltzmann relation: $n(W_1'') \simeq n_p \exp(V_A/V_t)$. These results thus confirm the validity of the usual assumption that in the so-called Shockley regime where the current is carried by diffusion in the base, the diffused-junction rectifier behaves exactly like a step-junction rectifier.

High-Level Condition: Since the quasi-neutrality condition, $n \simeq p$, applies under high-level condition, the analysis of the carrier distribution can proceed along the

[3] The solutions for this particular case have been given in [6] where they are compared with the well-known Sah–Noyce–Shockley theory of space-charge recombination.

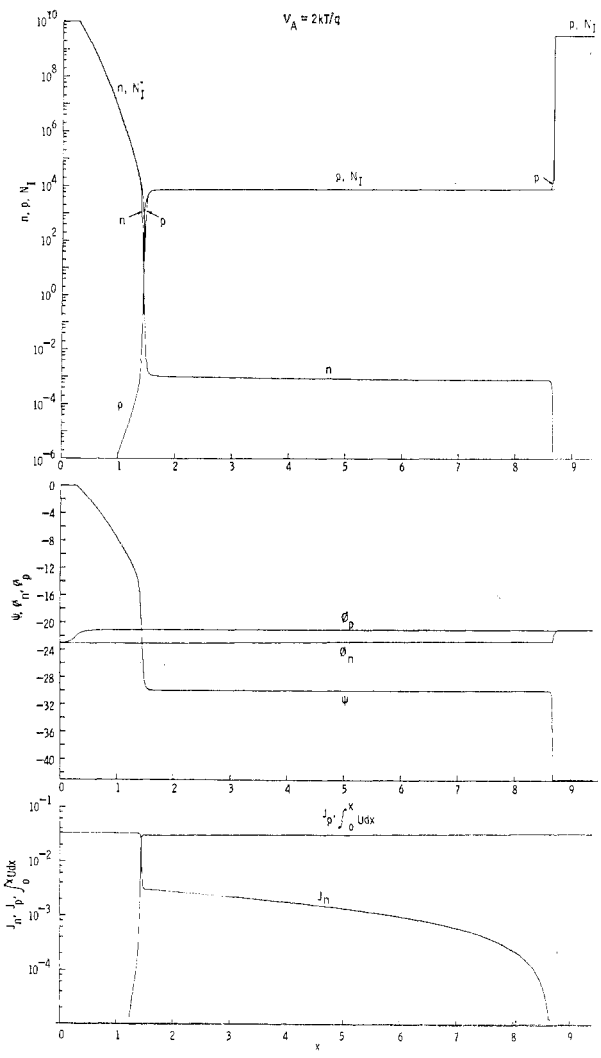

Fig. 2. Numerical solutions for the carrier concentrations, electrostatic potential, quasi-Fermi potentials, electron and hole current densities, and recombination rate integral at a forward bias of $2V_t$. All quantities are normalized according to Table II.

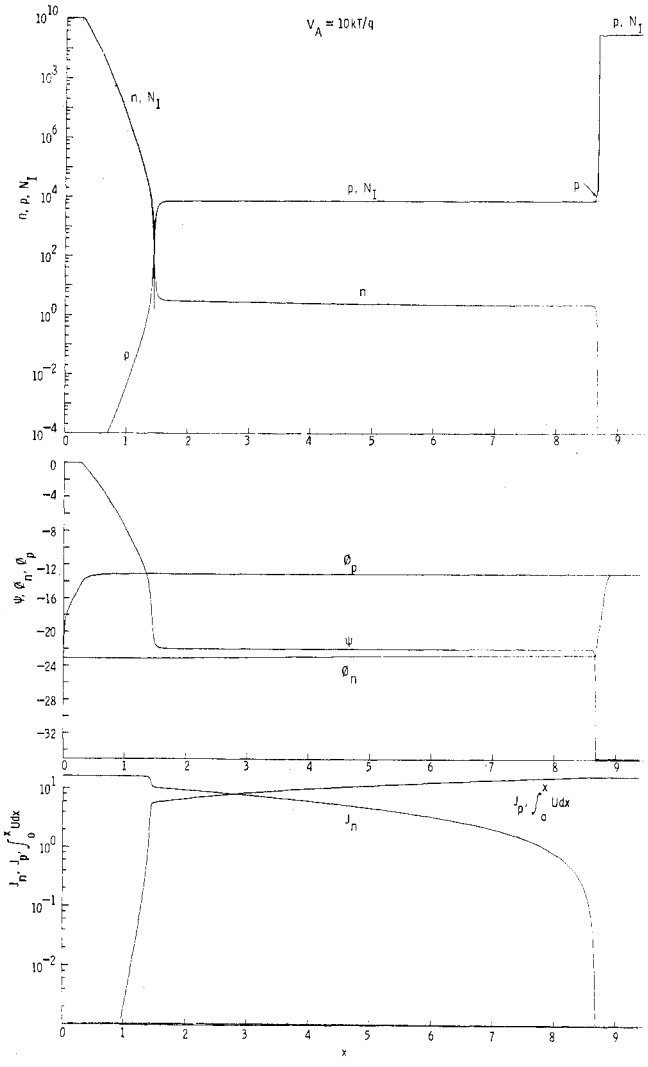

Fig. 3. Numerical solutions for the carrier concentrations, electrostatic potential, quasi-Fermi potentials, electron and hole current densities, and recombination rate integral at a forward bias of $10V_t$.

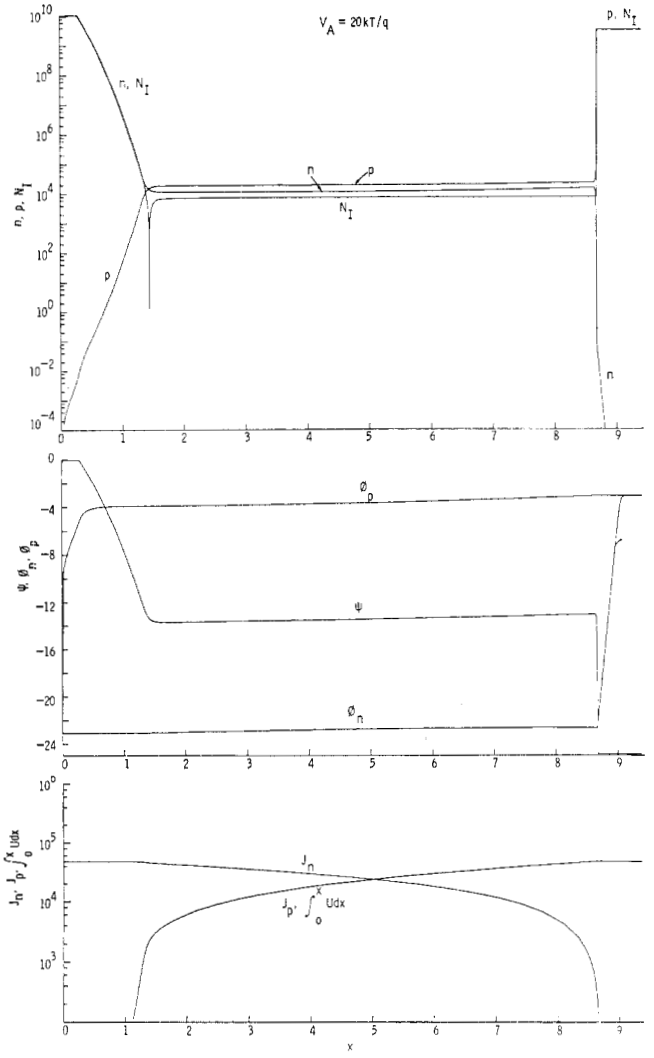

Fig. 4. Numerical solutions for the carrier concentrations, electrostatic potential, quasi-Fermi potentials, electron and hole current densities, and recombination rate integral at a forward bias of $20V_t$.

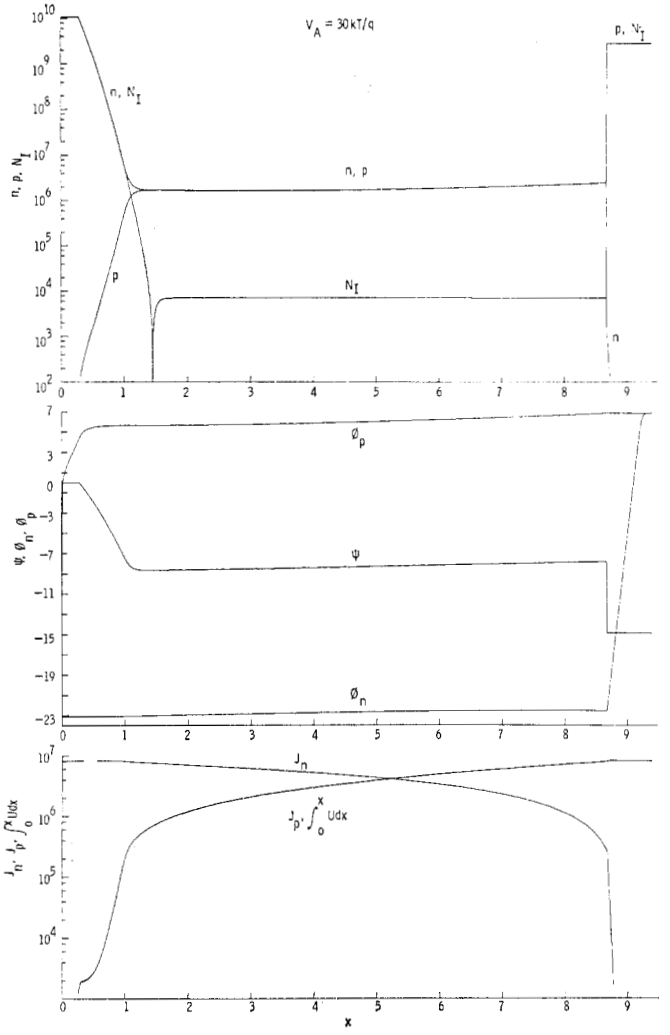

Fig. 5. Numerical solutions for the carrier concentrations, electrostatic potential, quasi-Fermi potentials, electron and hole current densities, and recombination rate integral at a forward bias of $30V_t$.

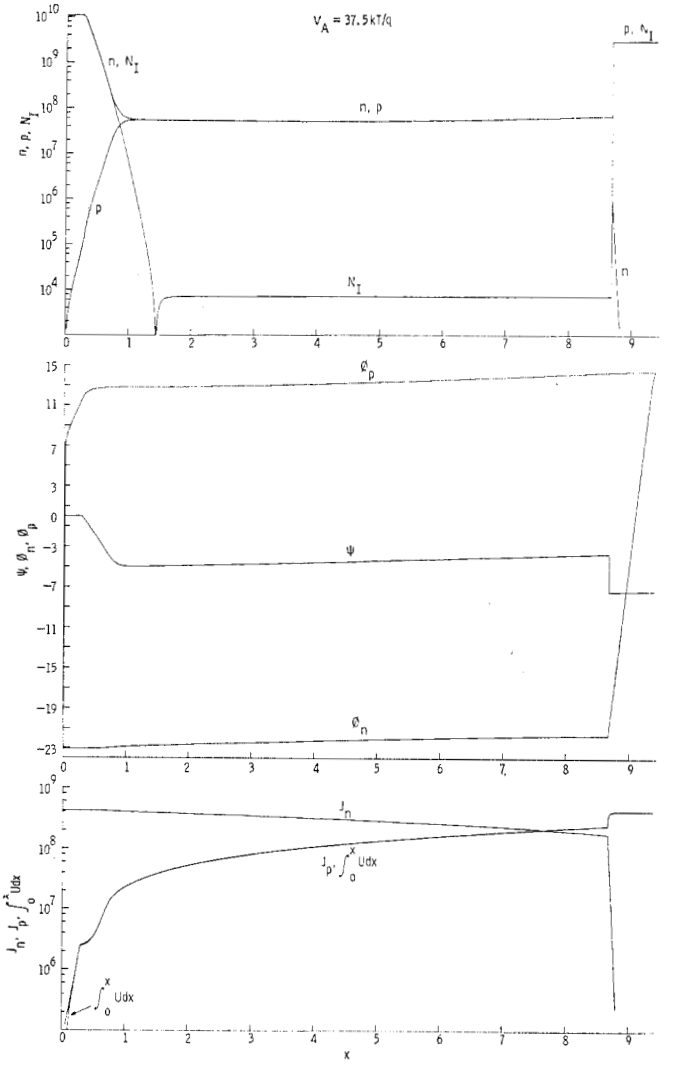

Fig. 6. Numerical solutions for the carrier concentrations, electrostatic potential, quasi-Fermi potentials, electron and hole current densities, and recombination rate integral at a forward bias of $37.5V_t$. Absence of carrier–carrier scattering is assumed.

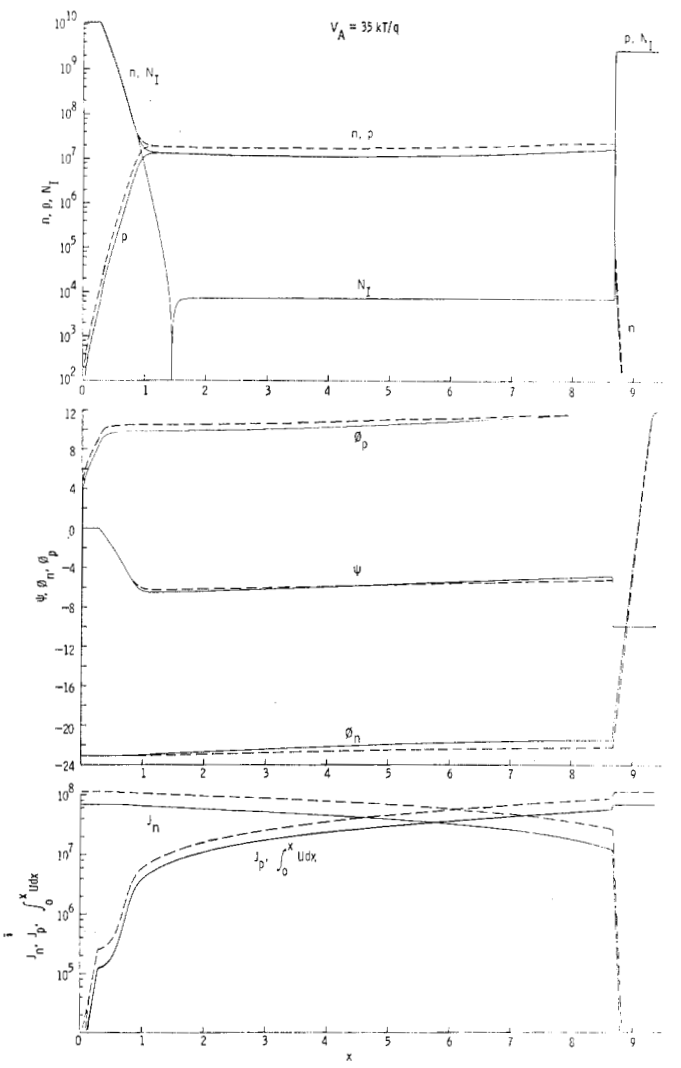

Fig. 7. Numerical solutions showing the effects of c-c scattering at a forward bias of $35V_t$. The solid curves were obtained with c-c scattering taken into account, the dashed curves without c-c scattering.

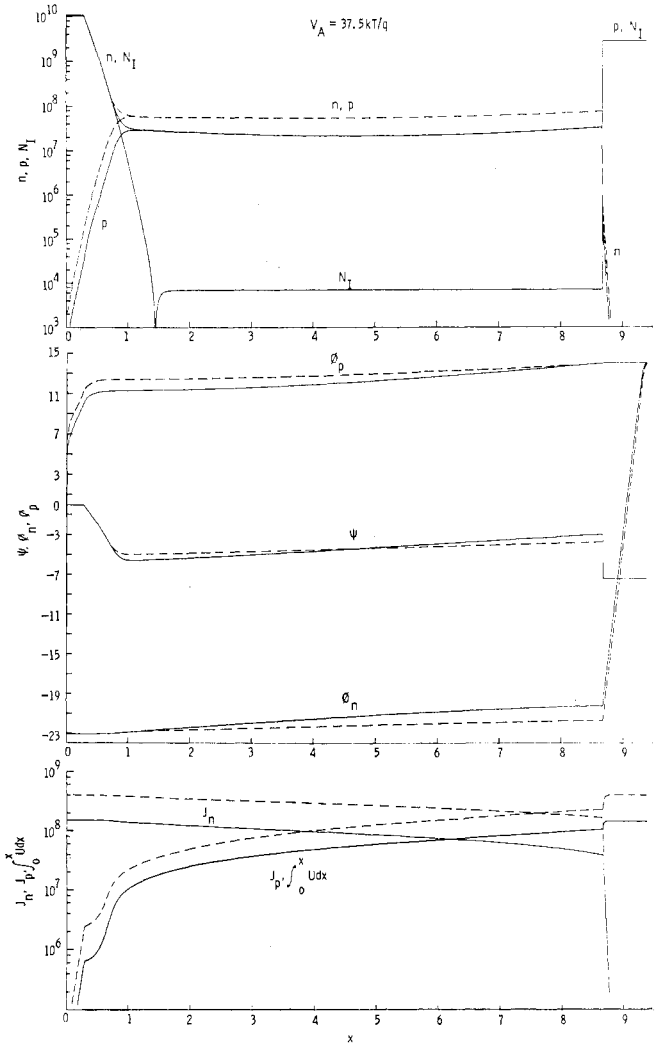

Fig. 8. Numerical solutions showing the effects of c-c scattering at a forward bias of $37.5V_t$. The solid curves were obtained with c-c scattering taken into account, the dashed curves without c-c scattering.

TABLE II

LIST OF NORMALIZATION FACTORS FOR THE QUANTITIES OF INTEREST

DESCRIPTION	NORMALIZED QUANTITY	NORMALIZATION FACTOR	
		symbol	numerical value
distance	x	$L_D \triangleq (\epsilon V_t/qn_i)^{1/2}$	3.45706×10^{-3} cm
time	t	L_D^2/D_0	1.19512×10^{-5} s
electrostatic potential	ψ	V_t	0.025875 V
applied voltage	V_A	V_t	"
barrier potential	ψ_d	V_t	"
carrier densities	n, p	n_i	1.4×10^{10} cm^{-3}
net impurity, donor, and acceptor densities	N_I, N_D, N_A	n_i	"
total, electron, and hole current densities	J_t, J_n, J_p	$-qD_0n_i/L_D$	-6.48784×10^{-7} A/cm^2
generation-recombination rate	U	D_0n_i/L_D^2	1.17142×10^{15} cm^{-3}s^{-1}
carrier diffusion coefficients	D_n, D_p	D_0	1 cm^2/sec
carrier mobilities	μ_n, μ_p	D_0/V_t	38.6473 cm^2/V·s

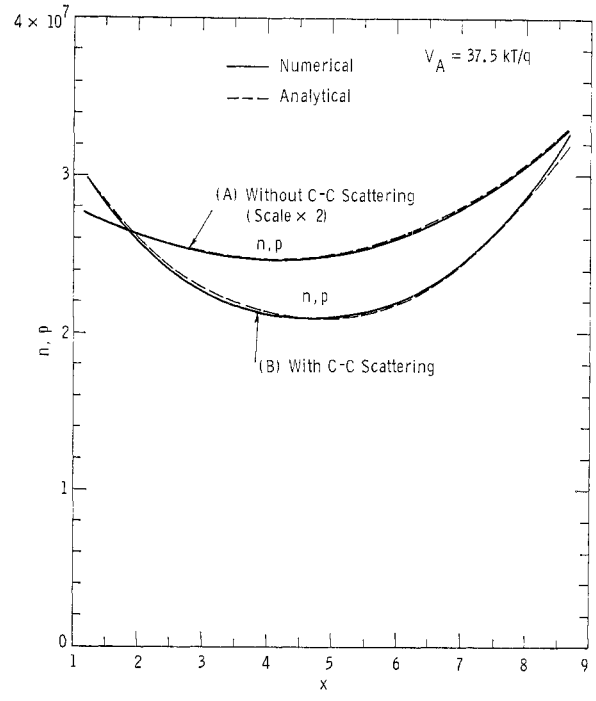

Fig. 9. Carrier distributions in the effective base region at a forward bias of $37.5V_t$ for case (A), without c-c scattering, and case (B), with c-c scattering. The dashed curves were calculated from (9).

same lines as in the case of the step-junction rectifier, using the well-known ambipolar diffusion solutions. The added complication here is that the effective basewidth increases with the injection level, although for the particular structure under consideration this increase is small compared to the total basewidth. To verify that the ambipolar diffusion equation is indeed applicable, the numerical solutions for a high-level case are compared in Fig. 9 to the following analytical solution to this equation [4]:

$$n(x) = \frac{J_b\tau}{2qL_a}\left\{\frac{\cosh\left[(x - W_{1/2})/L_a\right]}{\sinh\left[(W_2' - W_1')/L_a\right]} + B'\frac{\sinh\left[(x - W_{1/2})/L_a\right]}{\cosh\left[(W_2' - W_1')/L_a\right]}\right\} \quad (9)$$

where

$$J_b = q\int_{W_2'}^{W_1'} U \cdot dx \quad (10)$$

$$\tau = \tau_{n0} + \tau_{p0} \quad (11)$$

$$L_a^2 = 2V_t\tau/(\mu_n^{-1} + \mu_p^{-1}) \quad (12)$$

$$W_{1/2} = (W_1' + W_2')/2 \quad (13)$$

and

$$B' = [BJ_t + J_p(W_1') - J_n(W_2')]/J_b. \quad (14)$$

In the computation of the above analytical solution, values for the hole and electron current densities, $J_p(W_1')$ and $J_n(W_2')$, at the edges of the effective base region as well as the width $(W_2' - W_1')$ of this region,

were taken from the exact numerical solutions. Because there is no sharp boundary between the base and the diffused region, we have simply defined the location of $x = W_1'$ as the position where n and p have converged to within 1 percent of one another. This definition, though arbitrary, has proven satisfactory for purposes of all our analytical calculations.

The above solution was derived under the assumption of constant mobilities and constant lifetime. This assumption was justified in case (A) of Fig. 9 where c-c scattering effects are ignored; but, for this to apply in case (B) with c-c scattering, it was necessary to use, in place of a spatially varying c-c scattering mobility, the approximation of a constant mobility corresponding to the averaged carrier concentration in the base [19].

As can be seen from Fig. 9, the agreement between the numerical and analytical solutions is excellent in case (A). It is still satisfactory in case (B), despite the use of an average c-c scattering mobility.

A conclusion to be drawn from the above results is that, once we know how to calculate $J_p(W_1')$ and $J_n(W_2')$ analytically, the task of developing an analytical theory for the diffused-junction rectifier is essentially done.

P^+ Region

The calculation of $J_n(W_2')$ is equivalent to that of $J_n(W_2^*)$, since for the recombination parameters used, the recombination current in the space-charge region of the p^+-p junction is negligible for all bias conditions. The numerical solutions show that except for injected carrier concentrations exceeding 10^{16} cm^{-3} when c-c scattering comes into play, the carrier distributions follow in all cases studied the classical exponential type of behavior, and $J_n(W_2')$ is accurately given by

$$J_n(W_2') = q[n(W_2')^2/P^+][\exp (W_2 - x)/L_n]. \quad (15)$$

Diffused N^+ Region

As pointed out earlier, the behavior of the diffused junction at low forward bias has been analyzed elsewhere [6]. Our principal concern in this section is with the characteristics of the diffused region when the base is under high-level condition, and, in particular, with factors which determine $J_p(W_1')$. As can be seen from Figs. 5–8, $J_p(W_1') = q\int_0^{W_1'} U \cdot dx$, which suggests that we should begin our analysis of the diffused region by analyzing the behavior of $U(x)$.

The numerical solutions for $U(x)$ in the diffused region are shown in Fig. 10 for $V_A = 30$, 35, and $37.5\,V_t$ in the presence of c-c scattering,[4] and it is interesting to note that all the curves go through a maximum before falling off almost exponentially in the low injection level portion of the diffused region, with a slope roughly given by the normalized built-in field, qE/kT. This situation is reminiscent of that dealt with by Sah, Noyce, and Shockley [20] who, in their treatment of space-charge recombination in a p-n junction, used a linear electrostatic potential function and obtained an exponential falloff for U with a slope identically equal to the slope of the potential function. Remembering that the basis of the Sah–Noyce–Shockley treatment is the assumption of constant quasi-Fermi potentials for holes and electrons across the space-charge region, it seems reasonable to expect that the behavior of U in our diffused region is also a consequence of the constant quasi-Fermi potentials noted earlier.

To find out if this is true, we first note that under the condition of constant quasi-Fermi potentials, we have

$$n(x)p(x) = n(W_1')^2. \quad (16)$$

If we now substitute this relation into the recombination rate equation (8), and make use of the fact that $n, p \gg n_i$, we find that

$$U(x) = \frac{n(W_1')}{\tau_{p0}[n(W_1')/p] + \tau_{n0}[p/n(W_1')]}. \quad (17)$$

The above equation indicates that U has a maximum when $p = n(W_1')\sqrt{(\tau_{p0}/\tau_{n0})}$, with a value given by

$$U_{\max} = \frac{n(W_1')}{2\sqrt{(\tau_{p0}\tau_{n0})}}. \quad (18)$$

Moreover, this maximum bears a simple relationship to the recombination rate $U(W_1')$ at $x = W_1'$, since

$$U(W_1') = n(W_1')/(\tau_{p0} + \tau_{n0}). \quad (19)$$

Hence,

$$\frac{U_{\max}}{U(W_1')} = \frac{(\tau_{p0} + \tau_{n0})}{2\sqrt{(\tau_{p0}\tau_{n0})}}. \quad (20)$$

From the numerical solutions, we find that for the three cases under consideration, $V_A = 30$, 35, and $37.5\,V_t$, the corresponding values of $n(W_1')$ are 1.63×10^6, 1.33×10^7, and 3.00×10^7, respectively. From (18), the calculated values of $U_{\max}$ are then as follows: 1.54×10^6, 1.26×10^7, and 2.83×10^7. These values are seen to be in good agreement with the numerical values shown in Fig. 10. From the same figure, we see also that the ratio $U_{\max}/U(W_1')$ is very nearly the same for all three cases shown, with a value of about 1.8, as predicted by (20).

We now carry the analytical calculations a step further by noting that in view of the nearly exponential decay of U as previously noted, a very crude estimate of $\int U \cdot dx$ over the entire diffused region can be obtained by writing it as follows:

[4] We have found that there is essentially no difference in the numerical solutions for $V_A = 30\,V_t$, whether with or without c-c scattering. The solutions for U shown in Fig. 10 for $V_A = 30\,V_t$ can therefore be derived directly from the plots of n and p in Fig. 5.

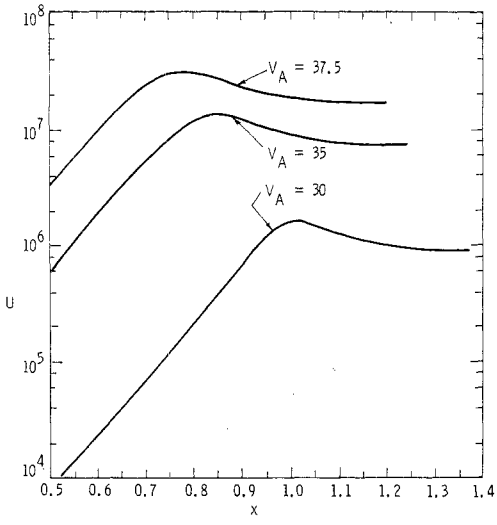

Fig. 10. Numerical solutions for the recombination rate in the diffused region at forward bias voltages of 30, 35, and $37.5V_t$, in the presence of c-c scattering.

$$\int U \cdot dx = 2U_{\max}(V_t/E) \tag{21}$$

where E is the average built-in field in the low-level injection or unmodulated portion of the diffused region, taken within a few units of (V_t/E) from the maximum shown in Fig. 10. The factor of 2 is used to account for some of the contribution from the region to the right of the maximum.

Then, substituting for $U_{\max}$ from (18), we obtain the following result:

$$J_p(W_1') = n(W_1')(V_t/E)/\sqrt{(\tau_{p0}\tau_{n0})}. \tag{22}$$

Note that the above equation gives a linear relationship between $J_p(W_1')$ and $n(W_1')$, as indicated by the numerical solutions in Figs. 5, 7, and 8. Moreover, the estimate that this equation provides for the value of $J_p(W_1')$ is found to be within a factor of 2 of the numerical solutions. This agreement is surprisingly good, in view of the very approximate nature of our analytical calculations. The real significance of these calculations, however, is that they provide us with an insight into the origin of the linear dependence of $J_p(W_1')$ on $n(W_1')$.

By employing an equally crude estimate for J_b, viz.,

$$J_b = qU(W_1')(W_2' - W_1') \tag{23}$$

we find that

$$\frac{J_p(W_1')}{J_b} = \frac{(\tau_{p0} + \tau_{n0})}{2\sqrt{(\tau_{p0}\tau_{n0})}} \frac{(V_t/E)}{(W_2' - W_1')} \tag{24}$$

which also explains why this ratio is nearly constant in all the high-level solutions.

Although the above treatment is based on the implicit assumption that the concentrations of recombination centers are the same in both the diffused region and the effective base region, (24) can still be used to give us some idea of what will happen when these concentrations are different. Consider, for example, the situation where throughout the graded-impurity region ($W_0 < x < W_1$), $\tau_{p0} = 2\times10^{-7}$ s and $\tau_{n0} = 2\times10^{-6}$ s, as compared to $\tau_{p0} = 2\times10^{-6}$ s and $\tau_{n0} = 2\times10^{-5}$ s in the p region ($W_1 < x < W_2$). Equation (24) leads us to expect that there will now be a substantial increase in $J_p(W_1')$, making it at least comparable to J_b. These expectations are borne out by the exact numerical solutions shown in Figs. 11 and 12. As can be seen from the figure, the ratios of $J_p(W_1')$ to J_b for $V_A = 30V_t$ and $37.5V_t$, obtained by using the new set of recombination parameters, are 0.54 and 0.59, respectively, as compared to ratios of 0.09 and 0.14, obtained by using the old set. However, the increase is not strictly proportional to the increase in the concentration of recombination centers in the diffused region, as we might expect from our simplified analysis. The main reason for this is that, with the new recombination parameters, there is a redistribution of the carrier concentrations in the effective base region, which makes the approximation of (24) now much worse than before.

The above numerical solutions, along with the analytical considerations, bring out an important consequence of the linear dependence of $J_p(W_1')$ on $n(W_1')$. It is that, if the number of recombination centers in the diffused region is substantially greater than in the base region, then the diffused junction would always have a low injection efficiency, regardless of the current or injection level. This is different from the situation in a step junction where the injection efficiency would be initially high and then degrade, as the current increases.

It is important to point out that the condition for the constancy of quasi-Fermi potentials or quasi-equilibrium in the diffused region is related to the type of impurity profile and the values of the recombination parameters that we used for this region. From our numerical solutions, we have found by varying the values of the recombination parameters that this condition is essentially equivalent to that established elsewhere [21] for a diffused region under low injection level conditions, namely,

$$E/V_t > 2/L_p \tag{25}$$

where E is the average built-in field and L_p the minority carrier diffusion length in the region. The reason for the applicability of the above criterion (25) is that our numerical solutions indicate that whenever deviations from quasi-equilibrium conditions set in, they generally occur in the low injection level portion of the diffused region rather than in the portion immediately next to the effective base region. A fuller discussion of these numerical solutions as well as of (25) will be given in Part II.

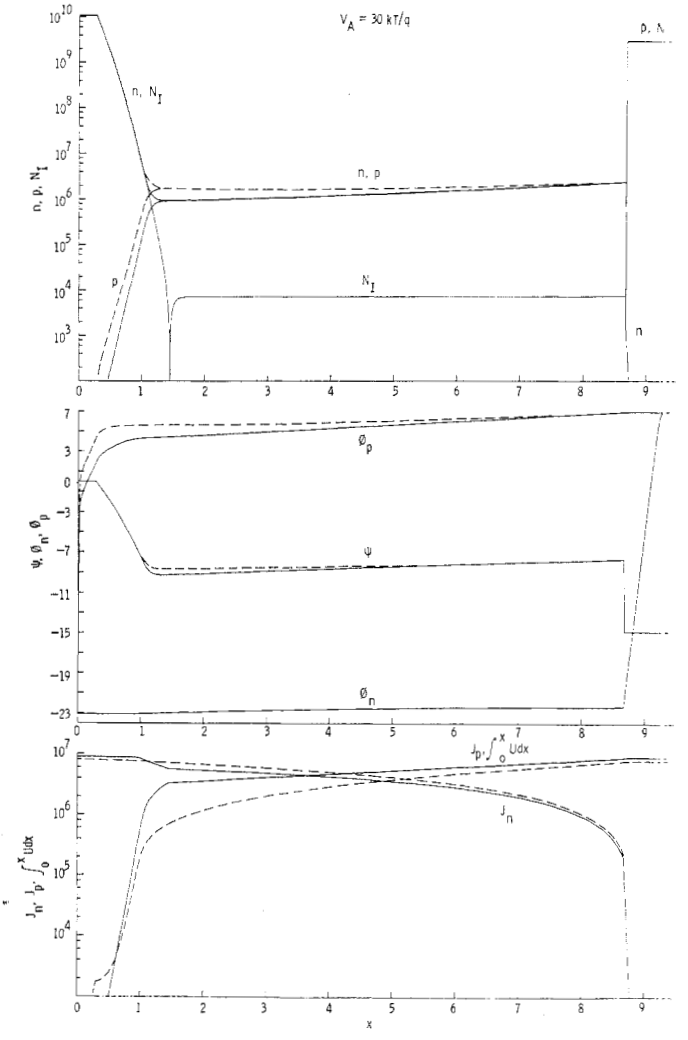

Fig. 11. Numerical solutions showing the effects due to an increase in the concentration of recombination centers in the diffused region relative to that in the p region at a forward bias of $30\,V_t$ in the presence of c-c scattering. The dashed curves were obtained for $\tau_{n0}=2\times10^{-5}$ s and $\tau_{p0}=2\times10^{-6}$ s in both the diffused and p regions, the solid curves for $\tau_{n0}=2\times10^{-6}$ s and $\tau_{p0}=2\times10^{-7}$ s in the diffused region ($W_0<x<W_1$) and $\tau_{n0}=2\times10^{-5}$ s and $\tau_{p0}=2\times10^{-6}$ s in the p region ($W_1<x<W_2$).

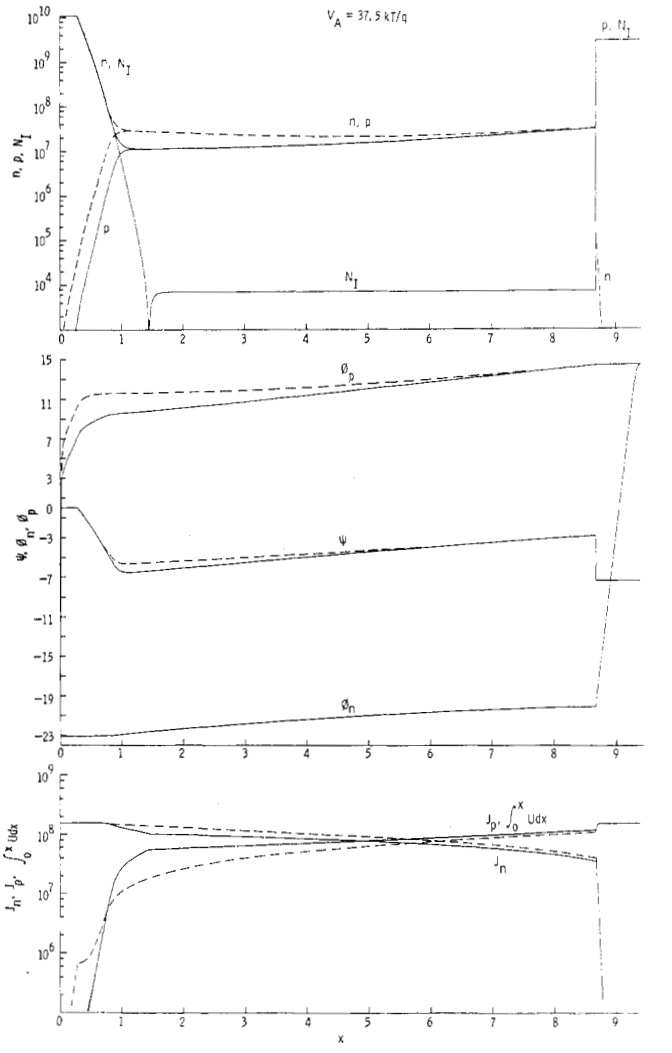

Fig. 12. Numerical solutions showing the effects due to an increase in the concentration of recombination centers in the diffused region relative to that in the p region at a forward bias of $37.5\,V_t$ in the presence of c-c scattering. The dashed curves were obtained for $\tau_{n0}=2\times10^{-5}$ s and $\tau_{p0}=2\times10^{-6}$ s in both the diffused and p regions, the solid curves for $\tau_{n0}=2\times10^{-6}$ s and $\tau_{p0}=2\times10^{-7}$ s in the diffused region ($W_0<x<W_1$) and $\tau_{n0}=2\times10^{-5}$ s and $\tau_{p0}=2\times10^{-6}$ s in the p region ($W_1<x<W_2$).

Voltage Calculations

Up to now, our discussion of the internal behavior of the device has been centered on the problem of calculating the carrier concentration and current distributions. In order to complete this discussion, it is now necessary to turn our attention to the calculation of the voltage drops in the various regions. In so far as the step p^+-p junction is concerned, no special problem arises, since the conventional Boltzmann relation obviously applies, as is verified by the numerical solutions. In the case of the effective base region under high-level conditions, the voltage drop is a function of the total current, the carrier concentrations, and the mobilities, and is also given by an expression analogous to that in the step-junction rectifier (see [4, eqs. (29), (31)]).

However, the situation in the diffused region is new, although the relative constancy of the quasi-Fermi potentials that we noted earlier implies that the Boltzmann relations must in some way be applicable. To find out if this is so, we have plotted in Fig. 13 the quantity $\ln[n(x)/n(W_0)]$ for comparison with $\psi(x)-\psi(0)$, and as we can see, these two quantities are in reasonable agreement throughout the bias range considered. Some deviation does occur in the upper end of the bias range, but this deviation is small compared to the total applied voltage, and for voltage calculations, neglecting it would result in only a small error. We conclude therefore that provided we know $n(W_1')$, the potential barrier across the diffused region can also be calculated from a simple Boltzmann relation

$$\psi_{d1} = V_t \ln[N^+/n(W_1')]. \tag{26}$$

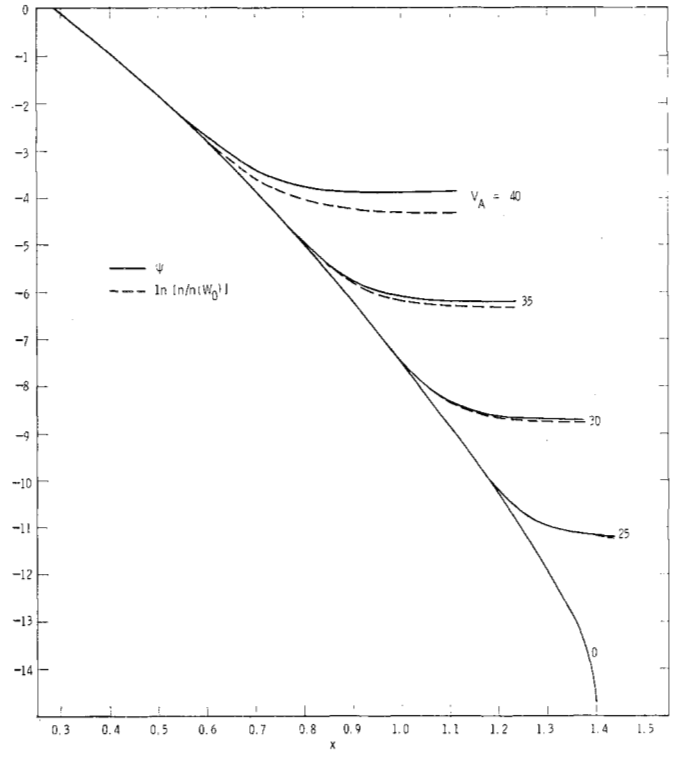

Fig. 13. Comparison of numerical solutions with Boltzmann relation for the majority carriers in the diffused region. Absence of c-c scattering is assumed. For a given forward bias, the deviation of the Boltzmann relation from the numerical solutions is greater in this case than if c-c scattering is allowed for.

J_t Versus V_A Characteristics

The current–voltage characteristics are shown in Fig. 14 for the range of bias voltages studied. The two curves given in the figure, curve (1) without c-c scattering and curve (2) with c-c scattering, were both obtained by assuming that the diffused region and the lightly doped base region have the same concentration of recombination centers.

As we have noted earlier, the characteristics at the lower end of the bias range are dominated by space-charge recombination at the diffused junction. However, the $J_t \propto \exp(V_A/2V_t)$ dependence usually associated with this particular mechanism is not observed, since before V_A is sufficiently large for this type of behavior to be well developed, the transition to the diffused-dominated or Shockley type of characteristics, with $J_t \propto \exp(V_A/V_t)$, has taken place. As can be seen from the figure, the Shockley regime is followed by a $J_t \propto \exp(V_A/2V_t)$ region corresponding to the onset of high-level injection in the base. In the case of curve (1), it is interesting to note that this region extends from $V_A \simeq 20V_t$ to $40V_t$ over a current range of more than 4 decades. The $\exp(V_A/2V_t)$ dependence is similar to the type of characteristics predicted by Hall for a step-junction p-i-n rectifier. However, Hall's theory was derived under the condition that the total current is accounted for by base recombination. While this condition holds

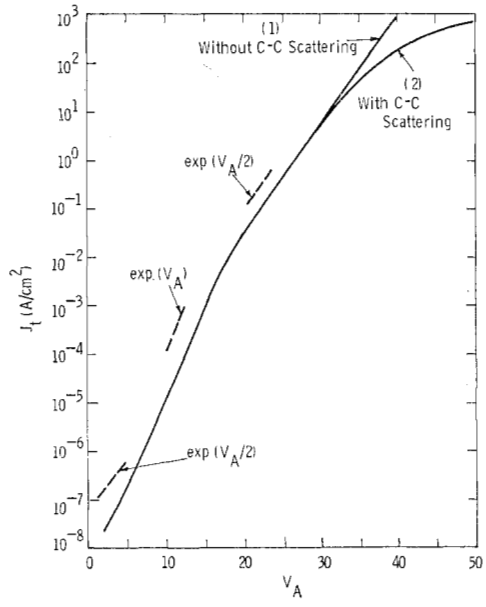

Fig. 14. Numerical solutions for the current–voltage characteristics for two cases. Curve (1): Without c-c scattering. Curve (2): With c-c scattering.

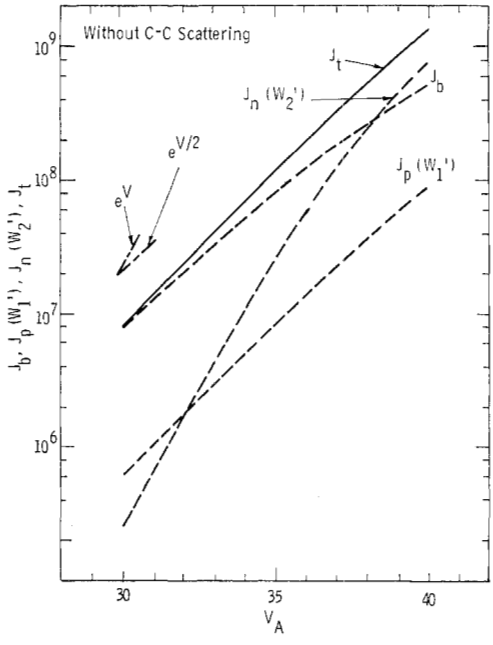

Fig. 15. Bias dependence of J_b, $J_p(W_1')$, and $J_n(W_2')$ in the absence of c-c scattering.

approximately for $V_A \lesssim 30V_t$, it does not apply at the higher voltages when the recombination current in the p^+ region becomes comparable to that in the base (cf., results for $V_A = 37.5V_t$ in Fig. 6).

The explanation for the large extent of the exp $(V_A/2V_t)$ region is given in Fig. 15, which shows the bias dependence of the three components of J_t, viz., J_b, $J_p(W_1')$ and $J_n(W_2')$. Around $30V_t$, $J_b \propto \exp[(V_{j1}+V_{j2})/2V_t]$ and $J_n(W_2') \propto \exp(2V_{j2}/V_t)$, and since $J_t \simeq J_b$ and $V_A \simeq V_{j1}+V_{j2}$, we have $J_t \propto \exp(V_A/2V_t)$.

At the higher bias voltages, although the same exponential dependence of J_b on $(V_{j1}+V_{j2})$ and $J_n(W_2')$ on V_{j2} continues to apply, we find that V_b is now no longer negligible. Moreover, it is increasing, largely at the expense of V_{j2}. This results in a slower rate of increase for both J_b and $J_n(W_2')$ with respect to V_A. However, the slower increase of J_b is almost exactly compensated by that of $J_n(W_2')$ so that we still have $J_t \propto \exp(V_A/2V_t)$.

It is also interesting to note from Fig. 15 that $J_p(W_1') \propto \exp(V_A/2V_t)$ throughout the bias range. This is due to the fact that $J_p(W_1') \propto n(W_1') \propto \exp(V_{j1}/V_t)$, and that V_{j1} changes at half the rate of V_A.

The bend in the characteristics due to c-c scattering, as shown by curve (2) in Fig. 14 can be explained along the same lines as those given above, i.e., in terms of the increase of V_b as the bias voltage is increased.

Conclusions

Exact numerical solutions have been obtained for a forward-biased diffused-junction n^+-p-p^+ rectifier operating from low to high injection levels. The results indicate that under high-level injection conditions, there exists a quasi-neutral ($n \simeq p$) region in the device which is not confined to the lightly doped p-base region alone but stretches into the diffused n^+ region as the injection level increases. For the particular impurity profile and the values of the Shockley–Read parameters that we used, we find additionally that the quasi-Fermi potentials for both electrons and holes are constant across a large portion of the diffused region adjoining the quasi-neutral or effective base region. The most interesting finding, however, is that, at the boundary between the effective base region and the diffused region, the hole current density varies directly as the carrier concentration, in contrast to the situation in a step-junction rectifier where the minority carrier current in the heavily doped regions varies as the square of the carrier concentration at the base edge. A simple analysis shows that this linear relationship can be related to the constant quasi-Fermi potentials across the diffused region.

As a consequence of the aforementioned linear relationship, the injection efficiency of the diffused junction is roughly independent of the injection or current levels. It may be high or low depending on whether the concentration of recombination centers in the diffused region is small or large compared to that in the base region. This is unlike the situation in a step junction where the injection efficiency would be initially high and then degrade, as the current increases.

Finally, by making a detailed comparison between the numerical solutions and the analytical approximations in the various regions in the device, we have laid the basis for the development of an approximate analytical theory for the diffused-junction rectifier.

Acknowledgment

The author would like to thank T. Seidman for devising the algorithm that solved the problem of recombination, A. Lavi and J. Koos for implementing the modified form of De Mari's algorithm in the early part of this work, and B. Kagle for programming both algorithms.

References

[1] R. N. Hall, "Power rectifiers and transistors," *Proc. IRE*, vol. 40, pp. 1512–1518, Nov. 1952.
[2] N. H. Fletcher, "The high current limit for semiconductor junction devices," *Proc. IRE*, vol. 45, pp. 862–872, June 1957.
[3] N. R. Howard and G. W. Johnson, "P+IN+ silicon diodes at high forward current densities," *Solid-State Electron.*, vol. 8, pp. 275–284, 1965.
[4] A. Herlet, "The forward characteristics of silicon power rectifiers at high current densities," *Solid-State Electron.*, vol. 11, pp. 717–742, 1968.
[5] S. C. Choo, "Numerical analysis of a forward-biased step-junction P-L-N diode," *IEEE Trans. Electron Devices*, vol. ED-18, pp. 574–586, Aug. 1971.
[6] ——, "Space-charge recombination in a forward-biased diffused p-n junction," *Solid-State Electron.*, vol. 14, pp. 1201–1208, 1971.
[7] R. G. Mazur and D. H. Dickey, "A spreading resistance technique for resistivity measurements on silicon," *J. Electrochem. Soc.*, vol. 113, pp. 255–259, Mar. 1966.
[8] D. L. Scharfetter and H. K. Gummel, "Large-signal analysis of a silicon Read diode oscillator," *IEEE Trans. Electron Devices*, vol. ED-16, pp. 64–77, Jan. 1969.
[9] L. W. Davies, "Electron-hole scattering at high injection levels in germanium," *Nature*, vol. 194, pp. 762–763, May 1962.
[10] W. Shockley and W. T. Read, "Statistics of the recombination of holes and electrons," *Phys. Rev.*, vol. 87, pp. 835–842, 1952. R. N. Hall, "Electron-hole recombination in germanium," *Phys. Rev.*, vol. 87, p. 387, 1952.
[11] R. A. Gudmundsen and J. Maserjian, Jr., "Semiconductor properties of recrystallized silicon in aluminum alloy junction diodes," *J. Appl. Phys.*, vol. 28, pp. 1308–1316, Nov. 1957.
[12] J. Burtscher, "Die Messung von Volumenströmen an Siliziumgleichrichtern. Eine neue Methode zur Ausschaltung der Oberflächeneinflüsse," *Solid-State Electron.*, vol. 12, pp. 591–604, 1969.
[13] H. K. Gummel, "A self-consistent iterative scheme for one-dimensional steady state transistor calculations," *IEEE Trans. Electron Devices*, vol. ED-11, pp. 455–465, Oct. 1964.
[14] A. De Mari, "An accurate numerical steady-state one-dimensional solution of the p-n junction," *Solid-State Electron.*, vol. 11, pp. 33–58, 1968.
[15] V. Arandjelovic, "Accurate numerical steady-state solutions for a diffused one-dimensional junction diode," *Solid-State Electron.*, vol. 13, pp. 865–871, 1970.
[16] T. I. Seidman and S. C. Choo, to be published.
[17] D. M. Caughey, "Simulation of UHF transistor small-signal behavior to 10 GHz for circuit modeling," in *2nd Biennial Cornell Elec. Eng. Conf.*, Ithaca, N. Y., 1969, pp. 369–379.
[18] For references, see R. W. Dutton and R. J. Whittier, "Forward current–voltage and switching characteristics of p^+-n-n^+ (epitaxial) diodes," *IEEE Trans. Electron Devices*, vol. ED-16, pp. 458–467, May 1969.
[19] S. C. Choo, "Effect of carrier lifetime on the forward characteristics of high-power devices," *IEEE Trans. Electron Devices*, vol. ED-17, pp. 647–652, Sept. 1970.
[20] C.-T. Sah, R. N. Noyce, and W. Shockley, "Carrier generation and recombination of *P-N* junctions and *P-N* junction characteristics," *Proc. IRE*, vol. 45, pp. 1228–1243, Sept. 1957.
[21] S. C. Choo, "The calculation of minority carrier current in diffused emitter regions," *Solid-State Electron.*, vol. 15, pp. 11–20, 1972.